APL Photonics

Epitaxial quantum dot lasers on silicon with high thermal stability and strong resistance to optical feedback

Cite as: APL Photonics **5**, 016103 (2020); https://doi.org/10.1063/1.5120029
Submitted: 15 July 2019 . Accepted: 18 December 2019 . Published Online: 07 January 2020

H. Huang, J. Duan, B. Dong, J. Norman, D. Jung, J. E. Bowers, and F. Grillot

COLLECTIONS

Paper published as part of the special topic on Hybrid Integration beyond Silicon Photonics
Note: This article is part of the Special Topic on Hybrid Integration Beyond Silicon Photonics.

View Online Export Citation CrossMark

ARTICLES YOU MAY BE INTERESTED IN

Tutorial on narrow linewidth tunable semiconductor lasers using Si/III-V heterogeneous integration
APL Photonics **4**, 111101 (2019); https://doi.org/10.1063/1.5124254

Real-time observation of the optical Sagnac effect in ultrafast bidirectional fibre lasers
APL Photonics **5**, 016104 (2020); https://doi.org/10.1063/1.5121723

Optical clearing and shielding with fan-shaped vortex beams
APL Photonics **5**, 016102 (2020); https://doi.org/10.1063/1.5133100

APL Photonics
Special Topic on Biomedical Photonics
READ NOW!

AIP Publishing

© 2020 Author(s).

Epitaxial quantum dot lasers on silicon with high thermal stability and strong resistance to optical feedback

Cite as: APL Photon. 5, 016103 (2020); doi: 10.1063/1.5120029
Submitted: 15 July 2019 • Accepted: 18 December 2019 •
Published Online: 7 January 2020

View Online Export Citation CrossMark

H. Huang,[1,a)] J. Duan,[1] B. Dong,[1] J. Norman,[2] D. Jung,[3,4] J. E. Bowers,[2,3,5] and F. Grillot[1,6]

AFFILIATIONS

[1]LTCI, Institut Polytechnique de Paris, Télécom Paris, 46 rue Barrault, 75013 Paris, France
[2]Materials Department, University of California Santa Barbara, Santa Barbara, California 93106, USA
[3]Institute for Energy Efficiency, University of California Santa Barbara, Santa Barbara, California 93106, USA
[4]Center for Opto-electronic Materials and Devices, Korea Institute of Science and Technology, Seoul 02792, South Korea
[5]Department of Electrical and Computer Engineering, University of California Santa Barbara, Santa Barbara, California 93106, USA
[6]Center for High Technology Materials, University of New-Mexico, 1313 Goddard St. SE, Albuquerque, New Mexico 87106, USA

Note: This article is part of the Special Topic on Hybrid Integration Beyond Silicon Photonics.
[a)]**Electronic mail:** heming.huang@telecom-paristech.fr

ABSTRACT

This work investigates the performance of 1.3-μm quantum dot lasers epitaxially grown on silicon under optical feedback sensitivity with different temperature and doping profiles. Experiments show that these quantum dot lasers exhibit a very high degree of resistance to both incoherent and coherent optical feedbacks. 10 Gbps penalty-free transmissions are also unveiled under external modulation and at different temperatures. The paper draws attention on quantum dot lasers with *p*-doping that exhibit a better thermal resistance, a lower linewidth enhancement factor, a higher critical feedback level, and a better spectral stability with less intensity noise. Together, these properties make epitaxial quantum dot lasers with *p*-doping more promising for isolator-free and Peltier-free applications, which are meaningful for future high-speed photonic integrated circuits.

© 2020 Author(s). All article content, except where otherwise noted, is licensed under a Creative Commons Attribution (CC BY) license (http://creativecommons.org/licenses/by/4.0/). https://doi.org/10.1063/1.5120029

I. INTRODUCTION

Over the past decade, silicon (Si) photonics have been introduced to overcome the low efficiency and high energy consumption of metal wiring, in particular, for high-speed communication systems, optical interconnects, as well as board-to-board and chip-to-chip integrated circuits.[1–6] Although Si exhibits a strong index contrast with silica ($\Delta n \approx 2$) hence being an excellent candidate for an on-chip waveguide with strong light confinement, it cannot easily provide efficient light emission due to its indirect bandgap nature. To overcome this issue, many efforts have been devoted to fabricate integrated light sources[5,7–10] either by considering hybrid integration of III-V semiconductor materials on Si or through direct heteroepitaxy onto Si or even germanium (Ge).[11–13] While for the former, flip-chip or wafer bonding has already reported good performance,[14–16] it does not always allow making optical devices with enough compactness. In addition, such hybrid lasers remain quite sensitive to not only coherent optical feedback from parasitic back-reflections of the laser emission by the vertical grating couplers and the multiple passive and active interfaces/transitions between the III-V material and Si[17–19] but also to possible incoherent feedback originating from amplified spontaneous emission (ASE) noises generated by active building blocks such as semiconductor optical amplifiers (SOAs) or active waveguides that are often integrated in the same photonic integrated circuits (PICs).[20] Although on-chip optical isolators with high performance have been reported, they still suffer from non-negligible insertion loss and remain quite complicate to fabricate.[21,22] As such, the development of

© Author(s) 2020

feedback-insensitive transmitters is still a major objective for silicon photonics related applications.

In order to meet the aforementioned requirements, semiconductor lasers monolithically grown on Si wafers, with low-cost, high-yield, energy efficiency, and much better scalability, are still needed.[9] To this end, InAs/GaAs quantum-dot (QD) technology has been shown to be a promising solution for silicon integration. Owing to the discrete energy levels, InAs/GaAs QD lasers exhibit both a better thermal stability and lower threshold current density as compared to their quantum well (QW) counterparts, advantages that are in favor to reduce the energy per bit consumption.[23] Although the direct growth on Si leads to the formation of crystal defects such as threading-dislocations (TDs), QDs are semiconductor "atoms" having independent energy barriers, hence leading to carrier localization that makes the gain medium less sensitive to TDs in contrast to their QW counterparts.[5,8,9] Last but not least, InAs/GaAs QD lasers often behave as quasi-class A oscillators, hence showing stronger damping effects and a lower linewidth enhancement factor (α_H-factor).[24–26] Together, these features do contribute to enhance the laser stability against undesired optical feedback.[27,28] For instance, a prior work has reported on a 25 Gbps error-free transmission with an integrated InAs/GaAs QD laser transmitter onto a Si substrate without an optical isolator for core I/O applications.[29] A recent result has also shown a 12.5 Gbps error-free transmission with directly modulated 1.3 μm InAs QD lasers directly grown on silicon. The power penalty is found to be less than 1 dB after a 12-km transmission distance at 5 Gbps.[26] More recently, we focused on the feedback-insensitive aspects of Si-based InAs/GaAs QD lasers where a remarkable feedback tolerance up to −7.4 dB was reported including test-bed experiments under strong optical feedback, leading to 10 Gbps error-free transmission with external modulation.[27] In this paper, we go a step further by studying the influence of the *p*-doping in Si-based QD lasers on the thermal stability and the sensitivity to both coherent and incoherent optical feedback. The use of *p*-doping is known to significantly improve both high temperature lasing characteristics and reliability of QD lasers. In this article, we show that *p*-doping not only reduces the thermal sensitivity and the relative intensity noise (RIN), which are critical for noise-sensitive applications, but also impacts the reduction of the α_H-factor as well as the optical feedback sensitivity, which is of vital importance for future deployment of such lasers in integrated communication systems.

II. QD DEVICES

The laser material of target devices was grown on pieces from a 300 mm on-axis (001) GaP/Si template purchased from NAsP III/V, GmbH. The epilayer structure is schematically illustrated in Fig. 1.

First, a buffer was grown to filter dislocations through a combination of four cycles of thermal annealing from 400 °C to 700 °C and strained InGaAs filter layers. Details are presented in Ref. 12. The laser structure consists of 1400 nm $Al_{0.4}Ga_{0.6}As$ upper (*p*-type) and lower (*n*-type) cladding to provide electrical and optical confinement. The active region consists of five periods of *p*-modulation doped InAs dot-in-a-well layers with 2 nm $In_{0.15}Ga_{0.85}As$ below and 5 nm on top of the dots. The InAs dots were grown at 495 °C with a nominal thickness of 2.55 Ml at 0.113 Ml/s. The dot growth conditions were optimized to minimize inhomogeneous broadening

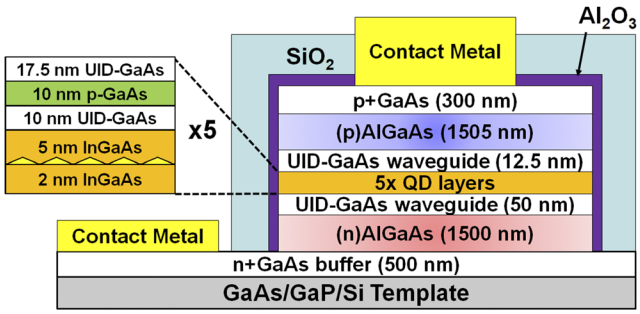

FIG. 1. Schematic descriptions of the QD laser epilayer structure (*p*-doped).

due to dot size fluctuations. To this end, each of the dot conditions (i.e., temperature, V/III ratio, deposition thicknesses, and compositions) were iteratively optimized due to the high degree of coupling between growth conditions. The dot layers were grown without strain coupling and with identical growth conditions to each other. The optimized growth conditions yielded a photoluminescence full-width-at-half-maximum of <30 meV. Each dot layer was separated by a 37.5 nm GaAs spacer, which included 10 nm of *p*-type material at a doping level of 5×10^{17} cm^{-3} for the *p*-doped device. As for the undoped one, the *p*-type layer is absent. These gain materials were also used in the studies described in Ref. 30. Further details of the epitaxy growth are available elsewhere.[8]

The studied laser devices were fabricated with standard dry etch and electron beam metal deposition techniques. The Fabry-Perot (FP) cavities of the lasers are measured at similar length, 1.1 mm for the undoped one and 1.35 mm for the other, with 3.5 μm wide ridges deeply etched (through the active region), and two top contacts were used for electrical injection. The facets were formed by cleaving after thinning the Si substrate to 200 μm. Dielectric facet coatings were then applied using ion beam deposition of repeated periods of SiO_2/Ta_2O_5 to give reflectivities of 60% (front) and 99% (rear).

Figure 2(a) depicts the power-current characteristics of both lasers at 293 K (room temperature). The threshold current for the

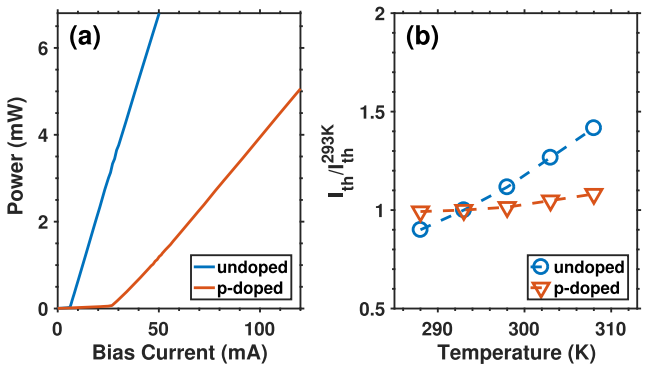

FIG. 2. (a) Light-current characteristics of the QD lasers at 293 K and (b) the temperature-relative variation of threshold currents compared to that at 293 K.

© Author(s) 2020

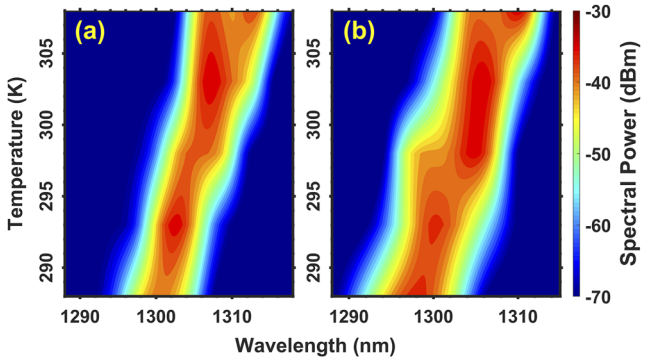

FIG. 3. Optical spectral envelopes of (a) undoped and (b) *p*-doped QD lasers at $3 \times I_{th}$ as a function of temperature.

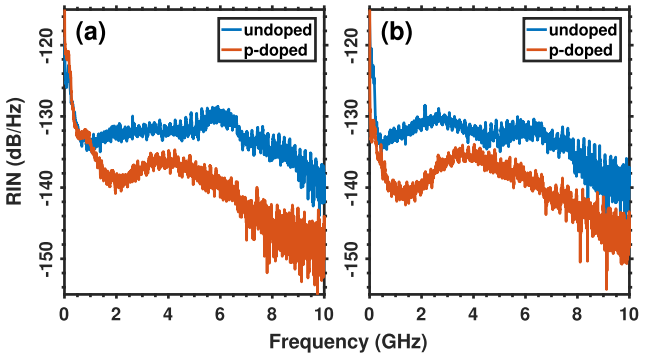

FIG. 4. Relative intensity noise (RIN) spectra of the QD lasers biased at $3 \times I_{th}$ for (a) 293 K and (b) 303 K.

undoped and *p*-doped devices is 6 mA and 26.5 mA, respectively. The higher threshold of the latter is attributed to the increased optical loss by high free carrier absorption that results from the large number of holes in the dots.[31,32] On the other hand, the inclusion of *p*-type doping contributes to eliminate gain saturation and to mitigate the thermal spread of holes,[33,34] hence leading to a rather temperature insensitive threshold current.[28,35–37] Such a feature is illustrated in Fig. 2(b), where the threshold currents, normalized to that at 293 K, are presented for the characterized temperature range from 288 K to 308 K. By comparison, one can easily note that while the *p*-doped device shows rather steady thresholds, the undoped one displayed a total variation of >60%. These results are coherent with previous studies.[28,38,39]

Figure 3 shows the optical spectral envelopes of the QD lasers at $3 \times I_{th}$ and for different temperatures. With or without doping, the center wavelength is found evenly red-shifted (10 nm), meaning that defects induced thermal effects are involved well above the laser threshold.

In order to better analyze the device operation well above threshold, the bias current used for both devices is maintained in what follows, if not specified, at $3 \times I_{th}$.

III. RELATIVE INTENSITY NOISE AND DYNAMICAL PROPERTIES

In order to measure the RIN of QD lasers, the laser emission is coupled into a lensed fiber and then the optical signal is converted into the electrical domain through a low-noise photodiode with a bandwidth of 10 GHz. The DC voltage is measured by a voltage meter through the DC monitor port of the photodiode, while the AC signal is amplified by a broadband amplifier with a typical small-signal gain of 30 dB. In the end, the amplified noise spectrum is measured on an electrical spectrum analyzer. It should be noted that the signal measured is only due to the fluctuation in carrier density, which caused the intensity noise. Indeed, even if the RIN can be limited by the shot noise resulting from the random occurrence of the photons, it remains usually much above that of the shot noise level, meaning that the measured noise spectrum from the detector reflects the contribution of carriers only.[40,41]

Figure 4 depicts the comparison of the measured RIN spectra between the undoped and *p*-doped lasers at 293 K and 303 K, with both lasers biased at $3 \times I_{th}$. At 293 K, a low RIN level of −140 dB/Hz at 10 GHz is demonstrated by the undoped device. While the laser is overdamped due to the absence of the relaxation oscillation frequency (ROF) peak whatever the bias current, it is worth nothing that the resonance peak at 6 GHz is not the ROF of the QD laser and rather results from the QD size dispersion induced impurity of longitudinal modes since it appears only at high bias current. In contrast, the *p*-doped QD laser exhibits a strong ROF peak at around 3.6 GHz due to a smaller damping factor with a reduced RIN level of −150 dB/Hz at 10 GHz. When further increasing the temperature from 293 K to 303 K, the ROF peak pops up at 2.6 GHz under the same bias level of $3 \times I_{th}$ for the undoped laser, suggesting that the damping of the laser is reduced. On the other hand, the RIN spectrum is more stable in the *p*-doped laser both in ROF peak and RIN level, indicating that the *p*-doping does contribute to improve the thermal stability. In what follows, both the ROF and damping factor are extracted from the curve-fitting of the RIN spectrum through the relationship

$$RIN(\omega) = \frac{a + b\omega^2}{(\omega^2 - \omega_{RO}^2)^2 + \omega^2\gamma^2}, \tag{1}$$

where ω_{RO} is the angular ROF, γ is the damping factor, ω is the angular frequency, a and b are the coefficients used for the curve-fitting.

Figure 5 shows the dynamic properties such as the damping factor as a function of the squared ROF for the undoped and *p*-doped lasers at 293 K and 303 K, respectively. In both cases, the evolution is linear following the relationship $\gamma = Kf_{RO}^2 + \gamma_0$ with K as the slope and γ_0 as the inverse of the differential carrier lifetime. For the undoped laser, a damping factor of 33 GHz at $3 \times I_{th}$ is extracted along with a K-factor of 4.7 ns and a ROF of 2.6 GHz at 293 K. The K-factor is reduced down to 3 ns at 303 K, leading to a smaller damping of 23 GHz and a decreased ROF of 2.4 GHz at $3 \times I_{th}$. By comparison, the damping factor of the *p*-doped laser is found at 25 GHz at $3 \times I_{th}$ with a K-factor of 1.5 ns and a ROF around 3.7 GHz. Once again, Fig. 5 shows that the *p*-doped QD laser is more stable with temperature. As far as direct modulation of light is concerned, these results confirm

© Author(s) 2020

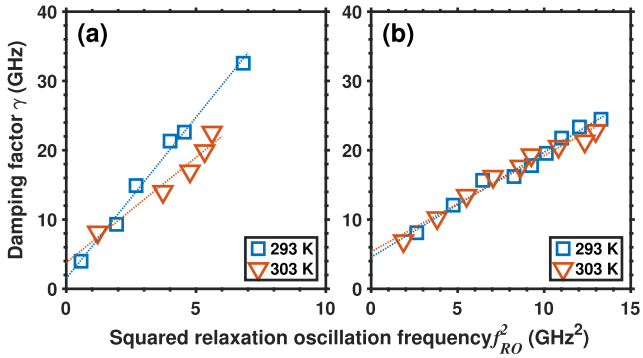

FIG. 5. The damping factor as a function of the squared relaxation oscillation frequency for (a) undoped and (b) *p*-doped QD laser devices.

that the introduction of *p*-doping can improve modulation capabilities, leading to both a higher ROF and a reduced damping factor. This effect was explained theoretically by the higher occupation of the QD hole levers leading to strong reduction of the hole scattering rates.[28]

IV. OPTICAL FEEDBACK SENSITIVITY

To further qualify the influence of *p*-doping on QD lasers subjected to optical feedback, this section is split into three parts: first, we remind the physical processes involved in the optical feedback and give some basic design rules for reaching feedback insensitive lasers; second, the impact of static optical feedback is studied without considering the modulation nor the transmission, hence allowing us to unveil how the optical feedback affects the spectral properties in both optical and radio-frequency (RF) domains; and in the last part, high-speed test bed experiments are performed with and without optical feedback. External modulation is preferred rather than direct modulation in order to keep the same degrees of freedom and avoid expanding the phase-space dynamics that would result in different feedback properties and the impossibility to properly compare the influence of the static optical feedback on the transmission performance.

The physical processes involved in a semiconductor laser under optical feedback are schematically described in Fig. 6. The phase-amplitude coupling in the active region between the returned light field and the intracavity is represented by field fluctuations both in amplitude and phase (i.e., $|\Delta E|$ and $\Delta\Phi$). Optical feedback is coupled into the laser cavity through the output facet and causes a perturbation on the photon density. As described by the rate equation model, this perturbation leads to a fluctuation of the carrier density and thus the optical gain.[42] The intensity fluctuation is then modulated by the damping effect and linked to the optical gain, where the gain variation itself impacts on the refractive index through the α_H-factor, hence leading to a shift in the lasing wavelength. On the other hand, the phase fluctuation caused by the returned field is related to wavelength fluctuation as well. The interaction of the intensity and phase loop essentially makes the dynamics of the laser system under optical feedback very complex and results in the severe complex laser instabilities such as coherence collapse.[42–44]

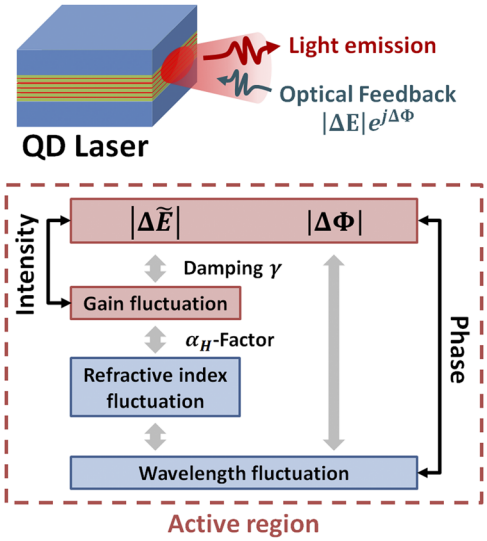

FIG. 6. Schematic representation of the physical processes involved in a semiconductor laser under optical feedback.

Figure 6 also gives insights into how to increase the resistance to optical feedback of the QD lasers. First, to reduce the coupling of the QD laser to the external world, a higher front facet reflectivity is preferred but doing so can also result in a strong reduction of the output power.[45] In this work, the power reflectivity of the front facet is fixed to 60%, which is enough to ensure good optical output power. Second, if the laser dynamics are heavily damped, the gain fluctuation introduced by the photon-density variation can be suppressed. Therefore, a large damping factor increases the optical feedback resistance of the laser that is exactly what happens with QD lasers. Note that even if *p*-doped QD lasers are less damped than the undoped ones, the value of the damping factor remains still beyond that of any bulk or QW lasers.[46] Third, decoupling the interaction between the intensity and phase loops is desired, in particular, by minimizing the α_H-factor. This is exactly what we previously reported with the *p*-doped QD lasers exhibiting a minimum value at threshold as low as 0.13.[27] Finally, longer cavities have large cavity photon roundtrip time and less change in the lasing wavelength for the same amount of phase fluctuation caused by the optical feedback. In this work, using an ~1-mm long cavity constitutes a good compromise for maintaining very good feedback resistance and high laser performance.

In the case of coherent optical feedback, a way of characterizing the optical feedback sensitivity is to estimate the critical feedback level for coherence collapse operation,[46]

$$r_{crit} = \frac{\tau_L^2\gamma^2}{16C^2}\left(\frac{1+\alpha_H^2}{\alpha_H^4}\right), \tag{2}$$

where τ_L is the photon cavity roundtrip time, γ is the damping factor, and C is the cavity coupling factor related to the facet reflectivity and equal to $(1-R)/2\sqrt{R}$ for FP lasers. As aforementioned, compared to QWs, one can expect an improvement of optical feedback resistance

© Author(s) 2020

in QDs, owing to the stronger damping and possibly the smaller α_H-factor. As in a real laser structure the propagating optical field penetrates into the cladding regions surrounding the active layer, the nominal value of α_H used in (2) should actually be expanded by $1 + \eta$ with $\eta = G\lambda/(2\pi n_e)$, where G is the material gain per unit length, λ is the lasing wavelength, and n_e is the effective index.[47] Taking into account that the material gain of the QD lasers under study is about a few hundreds of inverse centimeters, it is found that $\eta < 1$ and α_H should be pretty constant above threshold.[48,49] However, it is somewhat important to stress that this correcting factor remains minimalist in a sense that it does not incorporate the effects of the gain compression and the higher-energy states that are known to play a key role in the evolution of α_H with the bias conditions. In order to better illustrate this feature, α_H was also measured from I_{th} to $3 \times I_{th}$ at 293 K, as shown in Fig. 7. The dashed lines are for guiding eyes only. The first point at $I/I_{th} = 1$ on both curves are extracted with the standard ASE method,[30] whereas above threshold, values are captured using optical injection.[50] At $3 \times I_{th}$, the α_H-factor is found around 2 for the undoped laser, while it is still reduced down to 1.3 for the p-doped one. Using (2), the critical level for the p-doped laser is then found more than 4.2 dB above that of the undoped one and remains above whatever the pumping conditions since α_H and γ are not affected by the temperature variations.

A. Static optical feedback

Taking a practical approach, both coherent and incoherent optical feedback are considered in this section. In the former configuration, as the back-reflection originates from the laser itself, the influence is quantitatively investigated; while for the latter configuration, since the ASE noises are independent of the laser operating conditions, the affection of the feedback is qualitatively studied.

The setup to characterize the effects of the coherent optical feedback is schematically represented in Fig. 8. The emission from the QD laser front facet is coupled with an antireflection (AR) coated lensed fiber, and through the same interface, part of the light is reflected in the fiber back to the laser cavity from a distance of around 7 m away. The amount of return power is controlled and quantified by the feedback strength r_{ext}, defined

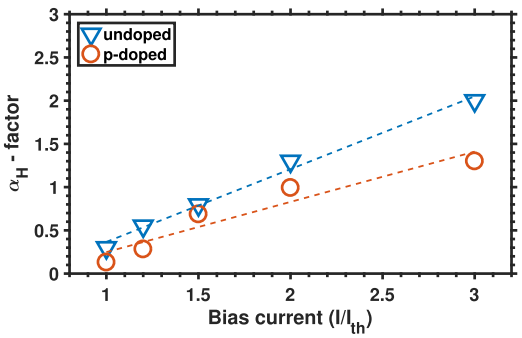

FIG. 7. The measured α_H-factor of both devices from I_{th} to $3 \times I_{th}$ at 293 K. The dashed lines are for guiding eyes only.

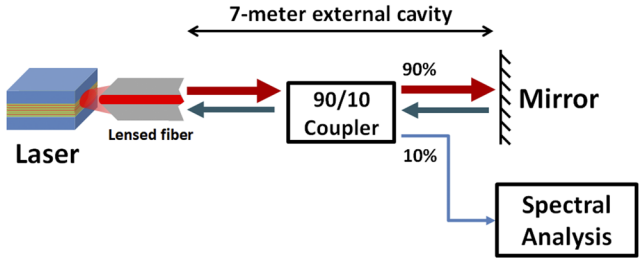

FIG. 8. Schematic representation of the coherent optical feedback setup.

as the ratio between the reflected power and free-space emitting power at the front facet. A polarization controller is inserted in the feedback path to make the reflected light polarization identical to that of the emitted light (transverse electric), namely, to maximize the effects of the optical feedback. As for the feedback phase, since the laser operated within the long-delay configuration where $f_{ext} \ll f_{ROF}$ with f_{ext} being the external cavity resonance frequency (14 MHz on this stage), the impact of the phase is negligible.[51] In our work, the achievable range of r_{ext} is from 0% to 16%. The remaining power is then sent to optical and electrical spectrum analyzers to monitor the spectral evolution as r_{ext} varies.

Figure 9 displays the corresponding feedback dynamics both in the radio-frequency (RF) and optical domains and for two different temperatures. The first column depicts the behaviors of the undoped QD laser, and the second column depicts those of the p-doped one. The lower temperature of 293 K is presented in the first and third rows, whereas the second and fourth rows correspond to 303 K. First, we focus on the upper half of the figure, where the four plots depict the RF spectral maps as a function of r_{ext}. As shown, whatever the feedback strength within the tested range, both lasers remain stable without developing any sign of nonlinear oscillations; hence, the RF spectral maps imply that both devices exhibit strong resistance to the back-reflections until the maximum feedback value of $r_{ext} = 16\%$ (−8 dB). Such a remarkable feature is attributed to several factors. First, the large damping effect that contributes to the suppression undamped relaxation oscillations. Second, the careful optimization of the inhomogeneous broadening related to QD size dispersion,[52] hence allowing to concentrate the lasing emission around the gain peak in order to maintain a reduced α_H-factor from threshold to above threshold. Finally, our prior works pointed out that a large excited-state to ground-state contrast ($I_{th}^{ES}/I_{th}^{GS} \gg 1$) lifts up the critical feedback level r_{crit}.[53] Here, with $I_{th}^{ES}/I_{th}^{GS} > 4.5$ for both devices, the results indicate a r_{crit} located beyond −8 dB, while any QW lasers typically exhibit a critical level below −25 dB.[27] Nevertheless, although the lasers maintain stable dynamics in the RF domain, they can display distinguishable behaviors in the optical domain. The lower half of Fig. 9 records the evolution of the main longitudinal FP mode for both temperatures as a function of the feedback strength. At 293 K, both QD devices remain stable with the increase in r_{ext}, namely, the FP modes are well preserved without spectral degradation. Only a slight red-shift is observed for the undoped laser when increasing the feedback strength. At 303 K, the two QD lasers behave quite differently. Although both do not

© Author(s) 2020

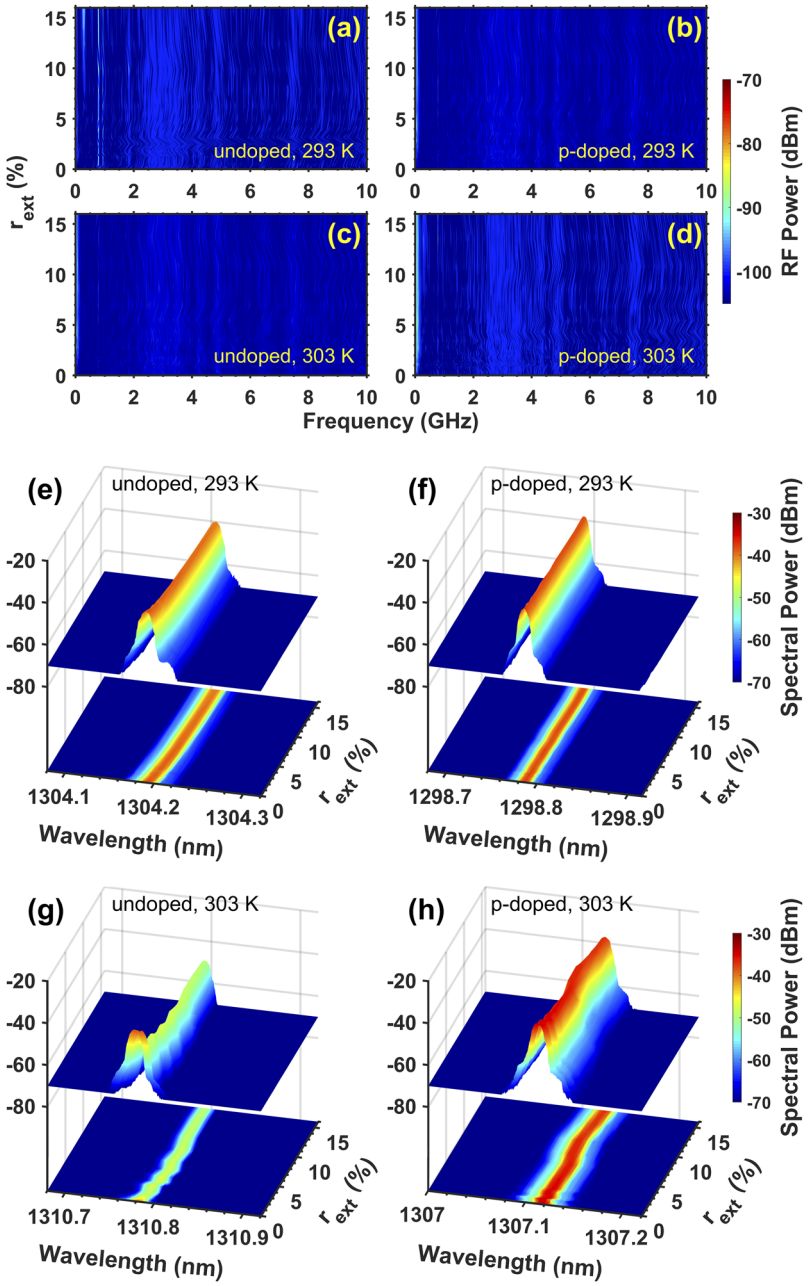

FIG. 9. RF and optical spectra for the main longitudinal mode as a function of r_{ext} in the undoped laser at 293 K [(a) and (e)] and 303 K [(c) and (g)], as well as in the *p*-doped laser at 293 K [(b) and (f)] and 303 K [(d) and (h)]. The bias current is fixed at $3 \times I_{th}$ for all subplots.

show coherence collapse operation, the undoped laser suffers from both intensity and wavelength fluctuations with the increment of r_{ext}, whereas the *p*-doped laser mostly exhibits wavelength fluctuations. Overall, the results suggest that the undoped laser has a lower tolerance to coherent optical feedback than the *p*-doped one. Such a discrepancy is explained twofold. First, as shown in Fig. 5, when increasing the temperature, the damping factor of the undoped laser exhibits a step down to a level below that of the *p*-doped one, hence leading to a reduction of the laser's feedback insensitivity. In addition, the α_H-factor of the undoped laser was found around 0.30 at 293 K and then to increase to 0.34 at 303 K, while it stays constant over temperature for the *p*-doped case[30] that remains also valid above threshold. Therefore, although the *p*-doped QD laser suffers from a higher threshold current, its better thermal stability leads to a more robust stability in the presence of coherence optical feedback.

To further illustrate the superior feedback tolerance of the *p*-doped device, we took a similar approach to realistic PIC

© Author(s) 2020

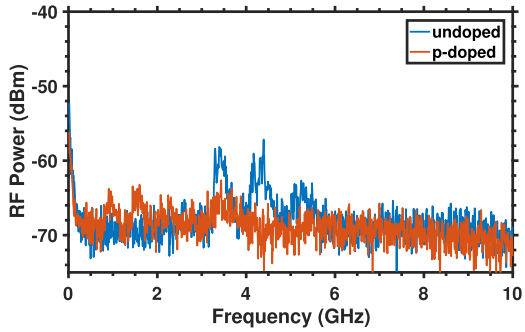

FIG. 10. RF spectra of the undoped laser and *p*-doped laser under maximal optical feedback in a much shorter cavity of about 10 cm. Both devices are biased at $3 \times I_{th}$ and operate at 293 K.

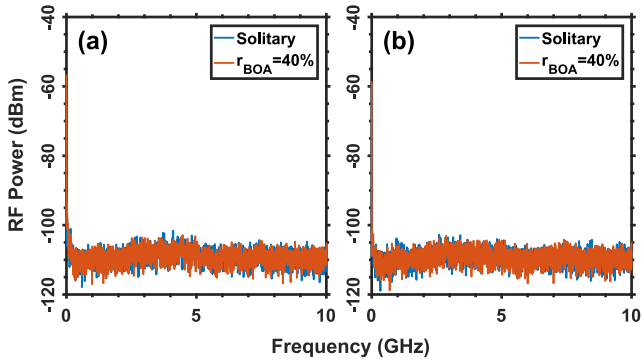

FIG. 12. RF spectra in free-running and under 40% incoherent feedback for (a) undoped and (b) *p*-doped lasers at $3 \times I_{th}$.

applications. To this end, we considered a situation for which both lasers are mounted in a shorter external cavity of about 10 cm in length, that is to say, a case where f_{ext} is on the same order as f_{ROF}. In such a way, enhanced feedback resonance can be expected. Figure 10 depicts the RF spectra of both devices operated at $3 \times I_{th}$ under r_{ext} ~ 16% with a temperature of 293 K. One can easily notice that while the undoped QD laser indeed gets slightly disturbed due to f_{ext}/f_{RO} ~ 1, the *p*-doped one demonstrates a remarkable spectral flatness, remaining almost unchanged, thanks to its lower linewidth enhancement factor, which is in good agreement with the aforementioned results.

As for the incoherent feedback case, the large span of ASE noises interferes with multiple cavity modes and hence can be destructive to the laser performance. To investigate how the QD lasers respond to such incoherent light, we used a booster optical amplifier (BOA) as a source of ASE noise, which is directly injected into the laser cavities through an optical circulator. The corresponding setup is depicted in Fig. 11. The QD lasers are maintained at 293 K under $3 \times I_{th}$. The strength of the ASE injection is controlled through the bias current onto the BOA and quantified using the ratio (r_{BOA}) between the power from the BOA that has reached the laser facet and the free-space power of the laser, i.e., similar to the definition of r_{ext}. At the end line, the spectral behaviors in both optical and RF domain are equally analyzed.

Figure 12 depicts the RF spectra of both devices in free-running and under incoherent optical feedback with r_{BOA} = 40%. For each laser, the two spectra are perfectly overlapped, implying a remarkable insensitivity against ASE noise. The results prove that these QD lasers exhibit a superior resistance to any kind of reflections such as those coming from other on-chip active building blocks. Note that in order to avoid any redundancy, only RF spectra are presented here. Indeed, as they do not display any characteristic frequencies in connection with external optical feedback, there is nothing more to expect from the optical spectra.

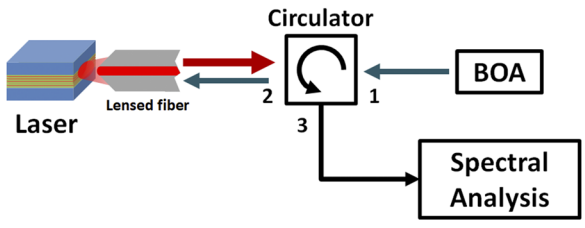

FIG. 11. Schematic representation of the incoherent optical feedback setup.

B. Test-bed experiments

The coherently fed-back laser source (from Sec. IV A) is now introduced to a fiberized transmission test-bed. The input light is modulated externally with a Mach-Zehnder modulator (MZM) at 10 GHz (on-off keying) with a pseudorandom binary sequence (PRBS) and a bit sequence length of $2^{31} - 1$. As aforementioned, external modulation is considered in order to keep the same degrees of freedom that would result in different feedback properties and the impossibility to compare static and dynamical optical feedback cases. Afterwards, the modulated optical signal is preamplified and transmitted through a 2 km single-mode fiber (SMF), as represented in Fig. 13. At the end, a variable optical attenuator (VOA) is used to tune the received power of the error detector in order to characterize the bit-error-rate (BER) performance.

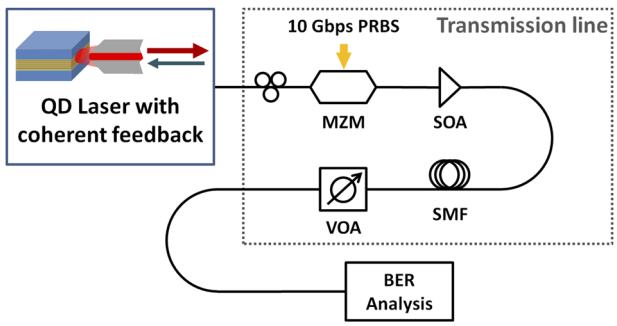

FIG. 13. Apparatus of the test-bed experiment. MZM: Mach-Zehnder modulator; SOA: semiconductor optical amplifier; SMF: 2 km long single mode fiber coil; VOA: variable optical attenuator.

© Author(s) 2020

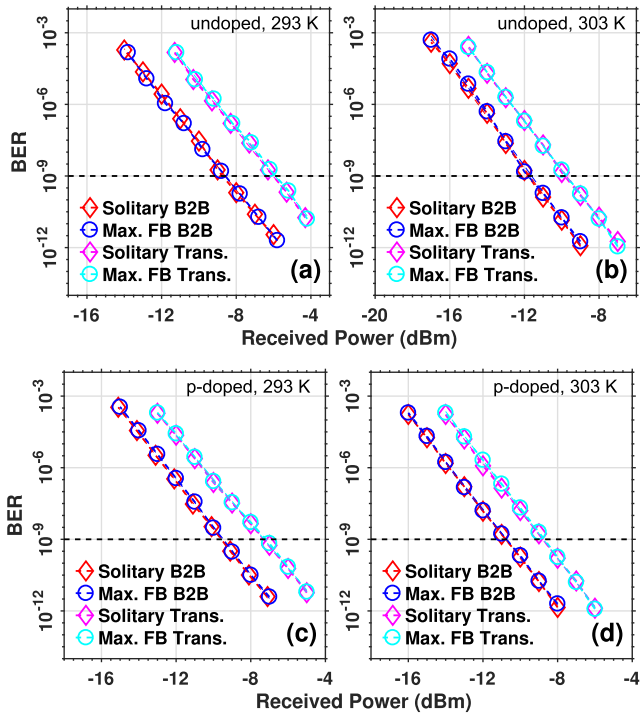

FIG. 14. BER plots for back-to-back (B2B) and after transmission (Trans.) with and without feedback (FB) for the undoped device at (a) 293 K and (b) 303 K and the *p*-doped device at (c) 293 K and (d) 303 K. The feedback level is at −8 dB, and the bias current is fixed at $3 \times I_{th}$.

Figure 14 depicts the BER plots in terms of received power for both the back-to-back configuration (red and blue) and after transmission (magenta and cyan) for four cases: undoped laser at (a) 293 K and (b) 303 K in free-running (square symbols) and under −8 dB maximal feedback (triangle markers) and *p*-doped laser at (a) 293 K and (b) 303 K in free-running and under maximal feedback (−8 dB). Whatever the configuration, BER plots between the free-running and the case for the highest feedback level (−8 dB) overlap each other, hence indicating an excellent stability in both lasers. Moreover, the temperature variation on this stage does not degrade the performances either; at 303 K, a BER in the order of 10^{-12} can still be achieved.

This exceptional feature showing no increase in the power penalty with the optical feedback is in line with the initial measurements of the relative intensity noise (RIN).[41] Given that the noise power received at the photodiode is directly proportional to the RIN such as $P_e \propto RS^2\Phi^2 RIN$ with R as the load resistance, S as the sensitivity of the photodiode, and Φ as the flux applied on the photodiode, one concludes that the power penalty of the QD lasers under study remains stable because the RIN itself is not enhanced by the optical feedback. Indeed, as the optical feedback increases the spontaneous emission in the laser cavity, the RIN scales up with the critical feedback level.[54] Because the QD lasers under study do not reach the critical feedback level, both the RIN and the power penalty remain constant which is an important statement for the realization of high performance communication systems.[44] On the top of that, the results also imply that our silicon-based QD lasers can also tolerate temperature fluctuation at least within the range under study. In addition, in all four subfigures, the power penalties after transmission are about 2 dB at the 10^{-9} BER level, which is due to the fiber chromatic dispersion and to residual ASE noises after the propagation through SOA. Let us stress out that due to limitation in equipment, the amplified signal was not filtered, meaning that residual ASE noises from the SOA should be considered through the fiber coil. On the other hand, looking side by side at Figs. 14(a) and 14(b), a shrink of the power penalty is observed. This can be explained by the wavelength difference between the laser emission and the SOA gain spectrum whose centered position is about 1310 nm. As the undoped laser precisely operates around 1310 nm (Fig. 9), the ASE noise level involved during the transmission is reduced, hence leading to a decrease in the power penalty. Overall, these results prove that both undoped and *p*-doped QD lasers directly grown on silicon exhibit superior insensitivity to external reflections with a higher thermal stability. Although these exceptional features remain both true for the QD laser with *p*-doping and within the range of temperature variations, it is however highly promising for the utilization of those optical sources in future photonics integrated circuits.

V. CONCLUSIONS

In this paper, both epitaxial undoped and *p*-doped QD lasers are found to exhibit a high tolerance to optical perturbations up to 16% (-8 dB) of light back reflected to the front facet. The degree of feedback tolerance of the QD gain medium is highly dependent on the dot size variations, but through careful optimization, this work shows how it is possible to minimize the inhomogeneous broadening. To this end, even epitaxial QD lasers on silicon can achieve high performance, suggesting their capability for isolator-free photonic integration. On the other hand, both devices have shown remarkable robustness against ASE noise that could distribute all over a real photonic integrated chip. In the end, the transmission test performed at 10 Gbps demonstrates a power penalty-free operation with both QD lasers even under the strongest optical feedback, hence indicating no RIN degradation. However, owing to its lower α_H-factor, we believe that the *p*-doped QD laser offers a higher potential for the three following reasons: (1) its critical feedback level is analytically predicted almost 5 dB higher than that of the undoped case and can be maintained constant with respect to the temperature; (2) the intensity noise, damping, and spectral purity are all much better than that of the undoped case especially over temperature variations; and (3) it shows a better stability to reflections coming from short distance. To sum, although the price to pay with *p*-doping is the higher threshold, the information displayed in this work show that, overall, the *p*-doped QD laser performs better even under optical feedback. When *p*-doping is properly optimized, a higher gain and a differential gain along with a reduced α_H-factor are achieved, hence improving high temperature lasing characteristics, reliability of QD lasers on silicon, as well as intensity noise feedback properties. We believe that the results presented in this work provide new physics and insights for the realization of future on-chip reflection insensitive and thermo-electrical-cooler-free transmitters. Further work will examine systematically the direct modulation configuration, wider temperature

© Author(s) 2020

variations, and short-delay optical feedback[55] and investigate distributed feedback (DFB) cavities. Based on the results reported here, researchers and engineers can make an informed judgement about which device would be the most suitable for a specific application.

ACKNOWLEDGMENTS

The authors acknowledge the financial support of ARPA-E (Grant No. DE-AR000067) and Institut Mines-Télécom. We thank Arthur Gossard and Mike Henry for valuable discussions.

REFERENCES

[1] V. R. Almeida, C. A. Barrios, R. R. Panepucci, and M. Lipson, "All-optical control of light on a silicon chip," Nature **431**, 1081–1084 (2004).
[2] M. Asghari and A. V. Krishnamoorthy, "Silicon photonics: Energy-efficient communication," Nat. Photonics **5**, 268–270 (2011).
[3] D. Liang and J. Bowers, "Recent progress in lasers on silicon," Nat. Photonics **4**, 511–517 (2010).
[4] Y. Arakawa, T. Nakamura, Y. Urino, and T. Fujita, "Silicon photonics for next generation system integration platform," IEEE Commun. Mag. **51**, 72–77 (2013).
[5] S. Chen, W. Li, J. Wu, Q. Jiang, M. Tang, S. Shutts, S. N. Elliott, A. Sobiesierski, A. J. Seeds, I. Ross, P. M. Smowton, and H. Liu, "Electrically pumped continuous-wave III-V quantum dot lasers on silicon," Nat. Photonics **10**, 307 (2016).
[6] K. Nishi, K. Takemasa, M. Sugawara, and Y. Arakawa, "Development of quantum dot lasers for data-com and silicon photonics applications," IEEE J. Sel. Top. Quantum Electron. **23**, 1–7 (2017).
[7] G.-H. Duan, C. Jany, A. L. Liepvre, A. Accard, M. Lamponi, D. Make, P. Kaspar, G. Levaufre, N. Girard, F. Lelarge, J.-M. Fedeli, A. Descos, B. B. Bakir, S. Messaoudene, D. Bordel, S. Menezo, G. de Valicourt, S. Keyvaninia, G. Roelkens, D. V. Thourhout, D. J. Thomson, F. Y. Gardes, and G. T. Reed, "Hybrid III-V on silicon lasers for photonic integrated circuits on silicon," IEEE J. Sel. Top. Quantum Electron. **20**, 158–170 (2014).
[8] D. Jung, J. Norman, M. J. Kennedy, C. Shang, B. Shin, Y. Wan, A. C. Gossard, and J. E. Bowers, "High efficiency low threshold current 1.3 μm InAs quantum dot lasers on on-axis (001) GaP/Si," Appl. Phys. Lett. **111**, 122107 (2017).
[9] J. Kwoen, B. Jang, J. Lee, T. Kageyama, K. Watanabe, and Y. Arakawa, "All MBE grown InAs/GaAs quantum dot lasers on on-axis Si (001)," Opt. Express **26**, 11568–11576 (2018).
[10] J. Kwoen, B. Jang, K. Watanabe, and Y. Arakawa, "High-temperature continuous-wave operation of directly grown InAs/GaAs quantum dot lasers on on-axis Si (001)," Opt. Express **27**, 2681–2688 (2019).
[11] Y.-G. Zhou, J. Duan, H. Huang, X.-Y. Zhao, C.-F. Cao, Q. Gong, F. Grillot, and C. Wang, "Intensity noise and pulse oscillations of an InAs/GaAs quantum dot laser on germanium," IEEE J. Sel. Top. Quantum Electron. **25**, 1–10 (2019).
[12] D. Jung, P. G. Callahan, B. Shin, K. Mukherjee, A. C. Gossard, and J. E. Bowers, "Low threading dislocation density GaAs growth on on-axis GaP/Si (001)," J. Appl. Phys. **122**, 225703 (2017).
[13] H. Liu, T. Wang, Q. Jiang, R. Hogg, F. Tutu, F. Pozzi, and A. Seeds, "Long-wavelength InAs/GaAs quantum-dot laser diode monolithically grown on Ge substrate," Nat. Photonics **5**, 416–419 (2011).
[14] G. Roelkens, L. Liu, D. Liang, R. Jones, A. Fang, B. Koch, and J. Bowers, "III-V/silicon photonics for on-chip and intra-chip optical interconnects," Laser Photonics Rev. **4**, 751 (2010).
[15] T. Katsuaki, W. Katsuyuki, and Y. Arakawa, "III-V/Si hybrid photonic devices by direct fusion bonding," Sci. Rep. **2**, 349 (2012).
[16] C. T. Santis, S. T. Steger, Y. Vilenchik, A. Vasilyev, and A. Yariv, "High-coherence semiconductor lasers based on integral high-Q resonators in hybrid Si/III-V platforms," Proc. Natl. Acad. Sci. U. S. A. **111**, 2879–2884 (2014).
[17] K. Schires, N. Girard, G. Baili, G. Duan, S. Gomez, and F. Grillot, "Dynamics of hybrid III-V silicon semiconductor lasers for integrated photonics," IEEE J. Sel. Top. Quantum Electron. **22**, 43–49 (2016).
[18] D. J. Lockwood and L. Pavesi, *Silicon Photonics II: Components and Integration* (Springer, 2011).
[19] D. Vermeulen, Y. D. Koninck, Y. Li, E. Lambert, W. Bogaerts, R. Baets, and G. Roelkens, "Reflectionless grating couplers for silicon-on-insulator photonic integrated circuits," Opt. Express **20**, 22278 (2012).
[20] Z. Zhang, H. Wang, N. Satyan, G. Rakuljic, C. T. Santis, and A. Yariv, "Coherent and incoherent optical feedback sensitivity of high-coherence Si/III-V hybrid lasers," in *Optical Fiber Communication Conference (OFC) 2019* (Optical Society of America, 2019), p. W4E.3.
[21] D. Huang, P. Pintus, and J. E. Bowers, "Towards heterogeneous integration of optical isolators and circulators with lasers on silicon [invited]," Opt. Mater. Express **8**, 2471–2483 (2018).
[22] Y. Zhang, Q. Du, C. Wang, T. Fakhrul, S. Liu, L. Deng, D. Huang, P. Pintus, J. Bowers, C. A. Ross, J. Hu, and L. Bi, "Monolithic integration of broadband optical isolators for polarization-diverse silicon photonics," Optica **6**, 473–478 (2019).
[23] G. Eisenstein and D. Bimberg, *Green Photonics and Electronics* (Springer, 2017).
[24] D. O'Brien, S. P. Hegarty, G. Huyet, J. G. McInerney, T. Kettler, M. Laemmlin, D. Bimberg, V. M. Ustinov, A. E. Zhukov, S. S. Mikhrin, and A. R. Kovsh, "Feedback sensitivity of 1.3 μm InAs/GaAs quantum dot lasers," Electron. Lett. **39**, 1819 (2003).
[25] F. Zubov, M. Maximov, E. Moiseev, A. Savelyev, Y. Shernyakov, D. Livshits, N. Kryzhanovskaya, and A. Zhukov, "Observation of zero linewidth enhancement factor at excited state band in quantum dot laser," Electron. Lett. **51**, 1686–1688 (2015).
[26] D. Inoue, D. Jung, J. Norman, Y. Wan, N. Nishiyama, S. Arai, A. C. Gossard, and J. E. Bowers, "Directly modulated 1.3 μm quantum dot lasers epitaxially grown on silicon," Opt. Express **26**, 7022–7033 (2018).
[27] J. Duan, H. Huang, B. Dong, D. Jung, J. C. Norman, J. E. Bowers, and F. Grillot, "1.3-μm reflection insensitive InAs/GaAs quantum dot lasers directly grown on silicon," IEEE Photonics Technol. Lett. **31**, 345–348 (2019).
[28] K. Lüdge, *Nonlinear Laser Dynamics: From Quantum Dots to Cryptography* (Wiley, 2012).
[29] K. Mizutani, K. Yashiki, M. Kurihara, Y. Suzuki, Y. Hagihara, N. Hatori, T. Shimizu, Y. Urino, T. Nakamura, K. Kurata, and Y. Arakawa, "Isolator free optical I/O core transmitter by using quantum dot laser," in *2015 IEEE 12th International Conference on Group IV Photonics (GFP)* (IEEE, Vancouver, Canada, 2015), pp. 177–178.
[30] J. Duan, H. Huang, D. Jung, Z. Zhang, J. Norman, J. E. Bowers, and F. Grillot, "Semiconductor quantum dot lasers epitaxially grown on silicon with low linewidth enhancement factor," Appl. Phys. Lett. **112**, 251111 (2018).
[31] M. Buffolo, F. Samparisi, C. De Santi, D. Jung, J. Norman, J. E. Bowers, R. W. Herrick, G. Meneghesso, E. Zanoni, and M. Meneghini, "Physical origin of the optical degradation of InAs quantum dot lasers," IEEE J. Quantum Electron. **55**, 1–7 (2019).
[32] M. Buffolo, F. Samparisi, L. Rovere, C. De Santi, D. Jung, J. Norman, J. E. Bowers, R. W. Herrick, G. Meneghesso, E. Zanoni, and M. Meneghini, "Investigation of current-driven degradation of 1.3 μm quantum-dot lasers epitaxially grown on silicon," IEEE J. Sel. Top. Quantum Electron. **26**, 1–8 (2020).
[33] D. G. Deppe, H. Huang, and O. B. Shchekin, "Modulation characteristics of quantum-dot lasers: The influence of *p*-type doping and the electronic density of states on obtaining high speed," IEEE J. Quantum Electron. **38**, 1587–1593 (2002).
[34] I. C. Sandall, P. M. Smowton, C. L. Walker, T. Badcock, D. J. Mowbray, H. Y. Liu, and M. Hopkinson, "The effect of *p* doping in InAs quantum dot lasers," Appl. Phys. Lett. **88**, 111113 (2006).
[35] G. Ozgur, A. Demir, and D. G. Deppe, "Threshold temperature dependence of a quantum-dot laser diode with and without *p*-doping," IEEE J. Quantum Electron. **45**, 1265–1272 (2009).
[36] O. Shchekin, J. Ahn, and D. Deppe, "High temperature performance of self-organised quantum dot laser with stacked *p*-doped active region," Electron. Lett. **38**(1), 712–713 (2002).
[37] K. Lüdge and E. Schöll, "Nonlinear dynamics of doped semiconductor quantum dot lasers," Eur. Phys. J. D **58**, 167–174 (2010).

© Author(s) 2020

[38]M. T. Crowley, N. A. Naderi, H. Su, F. Grillot, and L. F. Lester, "GaAs-based quantum dot lasers," in *Advances in Semiconductor Lasers*, edited by J. J. Coleman, A. Bryce, and C. Jagadish (Academic Press, 2012), pp. 371–417.
[39]J. C. Norman, Z. Zhang, D. Jung, C. Shang, M. Kennedy, M. Dumont, R. W. Herrick, A. C. Gossard, and J. E. Bowers, "The importance of *p*-doping for quantum dot laser on silicon performance," IEEE J. Quantum Electron. **55**, 1–11 (2019).
[40]Y.-G. Zhou, C. Zhou, C.-F. Cao, J.-B. Du, Q. Gong, and C. Wang, "Relative intensity noise of InAs quantum dot lasers epitaxially grown on Ge," Opt. Express **25**, 28817–28824 (2017).
[41]A. Y. Liu, T. Komljenovic, M. L. Davenport, A. C. Gossard, and J. E. Bowers, "Reflection sensitivity of 1.3 μm quantum dot lasers epitaxially grown on silicon," Opt. Express **25**, 9535–9543 (2017).
[42]J. Ohtsubo, *Semiconductor Lasers: Stability, Instability and Chaos*, Springer Series in Optical Sciences (Springer Berlin Heidelberg, 2010).
[43]D. Lenstra, B. Verbeek, and A. D. Boef, "Coherence collapse in single-mode semiconductor lasers due to optical feedback," IEEE J. Quantum Electron. **21**, 674–679 (1985).
[44]F. Grillot, B. Thedrez, O. Gauthier-Lafaye, M. F. Martineau, V. Voiriot, J. Lafragette, J. L. Gentner, and L. Silvestre, "Coherence collapse threshold of 1.3 μm semiconductor DFB lasers," IEEE Photonics Technol. Lett. **15**, 9–11 (2003).
[45]F. Grillot, G. H. Duan, and B. Thedrez, "Feedback sensitivity and coherence collapse threshold of semiconductor DFB lasers with complex structures," IEEE J. Quantum Electron. **40**, 231 (2004).
[46]L. A. Coldren, S. W. Corzine, and M. L. Mashanovitch, *Diode Lasers and Photonic Integrated Circuits*, Wiley Series in Microwave and Optical Engineering (Wiley, 1995).
[47]M. Osinski and J. Buus, "Linewidth broadening factor in semiconductor lasers—An overview," IEEE J. Quantum Electron. **23**, 9–29 (1987).
[48]Z. Zhang, D. Jung, J. C. Norman, P. Patel, W. W. Chow, and J. E. Bowers, "Effects of modulation *p* doping in InAs quantum dot lasers on silicon," Appl. Phys. Lett. **113**, 061105 (2018).
[49]Z. Zhang, D. Jung, J. Norman, W. W. Chow, and J. E. Bowers, "Linewidth enhancement factor in InAs/GaAs quantum dot lasers and its implication in isolator-free and narrow linewidth applications," IEEE J. Sel. Top. Quant. Electron **25**, 1–9 (2019).
[50]G. Liu, X. Jin, and S. L. Chuang, "Measurement of linewidth enhancement factor of semiconductor lasers using an injection-locking technique," IEEE Photonics Technol. Lett. **13**, 430 (2001).
[51]R. Tkach and A. Chraplyvy, "Regimes of feedback effects in 1.5-μm distributed feedback lasers," J. Lightwave Technol. **4**, 1655–1661 (1986).
[52]J. C. Norman, D. Jung, Y. Wan, and J. E. Bowers, "Perspective: The future of quantum dot photonic integrated circuits," APL Photonics **3**, 030901 (2018).
[53]H. Huang, J. Duan, D. Jung, A. Y. Liu, Z. Zhang, J. Norman, J. E. Bowers, and F. Grillot, "Analysis of the optical feedback dynamics in InAs/GaAs quantum dot lasers directly grown on silicon," J. Opt. Soc. Am. B **35**, 2780–2787 (2018).
[54]J. Wang and K. Petermann, "Noise analysis of semiconductor lasers within the coherence collapse regime," IEEE J. Quantum Electron. **27**, 3–9 (1991).
[55]T. Heil, I. Fischer, W. Elsäßer, and A. Gavrielides, "Dynamics of semiconductor lasers subject to delayed optical feedback: The short cavity regime," Phys. Rev. Lett. **87**, 243901 (2001).

© Author(s) 2020